Nanoscale

PAPER

View Article Online
View Journal | View Issue

Cite this: *Nanoscale*, 2019, **11**, 9053

Surface plasmon resonance enhanced direct Z-scheme TiO_2/ZnTe/Au nanocorncob heterojunctions for efficient photocatalytic overall water splitting†

Wenjun Zhang,[a] Yi Hu,[a] Changzeng Yan,[a] Daocheng Hong,[a] Renpeng Chen,[a] Xiaolan Xue,[a] Songyuan Yang,[a] Yuxi Tian,[a] Zuoxiu Tie[a] and Zhong Jin *[a,b]

Solar-driven photocatalytic overall water splitting is regarded as one of the ideal strategies to generate renewable hydrogen energy without the initiation of environmental issues. However, there are still a few remaining challenges to develop wide-light-absorption and stable photocatalysts for the simultaneous production of H_2 and O_2 in pure water without sacrificial reagents. Herein, we report the design and preparation of Z-scheme TiO_2/ZnTe/Au nanocorncob heterojunctions by homogeneously decorating Au nanoparticles onto the surface of core–shell TiO_2/ZnTe coaxial nanorods for highly efficient overall water splitting. With the appropriate band structure of TiO_2/ZnTe heterojunctions and the surface plasmon resonance enhancement of Au nanoparticles, the well-designed TiO_2/ZnTe/Au nanocorncob heterojunctions can synergistically make effective utilization of broad-range solar light illumination and enhance the separation efficency of electron–hole pairs, as evidenced by UV-Vis absorption and time-resolved photoluminescence spectroscopy. Photoelectrochemical characterization confirms that the water-splitting reaction on TiO_2/ZnTe/Au nanocorncobs is mainly carried out *via* a two-electron/two-electron transfer process with an intermediate product of H_2O_2. As a result, the TiO_2/ZnTe/Au nanocorncob photocatalyst can generate H_2 and O_2 with a stoichiometric ratio of 2 : 1 under light irradiation without any sacrificial agents, exhibiting a high H_2 production rate of 3344.0 μmol g^{-1} h^{-1} and a solar-to-hydrogen (STH) efficiency of 0.98%. Moreover, the TiO_2/ZnTe/Au nanocorncob heterojunctions show high stability and well-preserved morphological integrity after long-term photocatalytic tests. This study provides a prototype route to produce clean hydrogen energy from only sunlight, pure water, and rationally-designed heterojunction photocatalysts.

Received 4th March 2019,
Accepted 9th April 2019

DOI: 10.1039/c9nr01732a

rsc.li/nanoscale

Introduction

Solar driven water splitting for H_2 generation has drawn great attention, since the environmental pollution and energy crisis have become serious social issues. However, most photocatalytic systems employed for water splitting suffer from low efficiency, inferior stability, and high cost.[1–4] To solve these problems, it is a necessity to develop efficient photocatalysts based on Earth-abundant, non-toxic, stable and broad-light-absorption materials. TiO_2 as one of the most promising photocatalytic materials possesses excellent chemical- and photo-stability, and low cost as well as environmentally benign characteristics.[5] However, owing to its large bandgap (3.0–3.2 eV), TiO_2 is only capable of harvesting ultraviolet (UV) light, which corresponds to less than 5% of total solar energy. Moreover, the photocatalytic activity of TiO_2 is limited by rapid photo-induced carrier recombination.[6] To overcome these issues, many strategies have been adopted, such as constructing high-aspect-ratio nanostructures, loading dopants/sensitizers and decorating noble metal cocatalysts.[7,8] In particular, heterojunctions composed of TiO_2 and other narrow bandgap semiconductors (including $BiVO_4$,[9] Cu_2O,[10] WO_3 [11] or CdS[12]) have sprung up in recent years. As one model of heterojunctions, the direct Z-scheme system uses two compatible materials to mimic the natural photosynthesis process in plants to efficiently generate hydrogen and oxygen separately.[13–16] The Z-scheme system makes use of solar energy harvested by two different light absorbers and extends the decay lifespan of photo-induced carriers, which may potentially lead to high photocatalytic activity. Therefore, it is attractive to construct an effective Z-scheme photocatalytic system

[a]*Key Laboratory of Mesoscopic Chemistry of MOE, School of Chemistry and Chemical Engineering, Nanjing University, Nanjing, Jiangsu 210023, China.*
E-mail: zhongjin@nju.edu.cn
[b]*Shenzhen Research Institute of Nanjing University, Shenzhen 518063, China*
†Electronic supplementary information (ESI) available. See DOI: 10.1039/c9nr01732a

based on TiO_2 and another suitable semiconductor material that can satisfy the specific requirements of band edge matching and Ohmic contact.[17]

Nanostructural semiconductors, such as ZnO,[18,19] ZnS,[20,21] CdS,[22] CdSe,[23] WS_2 [24] and ZnTe,[25,26] have been investigated in the photocatalysis field. Although being employed for fabricating solar cells,[27] green light-emitting diodes[28] and optoelectronic devices,[29,30] ZnTe has not attracted great attention to act as a photocatalyst for water splitting. ZnTe has a direct band gap of approximately 2.26 eV,[31] which can enhance the photocatalytic activity by absorbing sufficient solar light. Nevertheless, most studies have concentrated on ZnTe solely in the photocatalysis field, rather than in tandem with TiO_2 as a Z-scheme heterojunction.

Herein, we report a rationally designed photocatalyst by decorating Au nanoparticles homogeneously on the surface of core–shell TiO_2/ZnTe nanorod heterojunctions (TiO_2/ZnTe/Au nanocorncobs) for high-efficiency photocatalytic overall water splitting without the need for sacrificial reagents. The TiO_2/ZnTe coaxial nanorod heterojunction possesses a high aspect ratio and broad light absorption range. The built-in electric field at the interfaces of TiO_2/ZnTe nanorods provides a "highway" for photo-generated carrier transport/separation.[32] Moreover, Au nanoparticles with a strong surface plasmon resonance (SPR) effect[33] and electron collective ability synergistically enhance the sunlight utilization and effective electron–hole separation. As a result, TiO_2/ZnTe/Au nanocorncob heterojunctions exhibit high H_2 and O_2 evolution rates, improved solar-to-hydrogen (STH) efficiency and good performance stability under light illumination in pure water.

Experimental

Preparation of ultrathin TiO_2 nanowires

Briefly, 0.64 g of anatase TiO_2 powder (purchased from Shanghai Mindray Chemistry Technology Co.) was dissolved in 75 mL of 10 M KOH solution under stirring and moved into a 100 mL Teflon-lined autoclave. The autoclave was sealed and heated to 130 °C for 2 days to obtain white potassium titanate nanowires. The nanowires were collected by centrifugation and washed with deionized water and ethanol several times and dried at 60 °C overnight under vacuum. Subsequently, 0.2 g of the as-prepared potassium titanate nanowires were dispersed in 40 mL of deionized water, and homogeneously mixed with 50 mL of 0.05 M Urotropin (HMTA, Beijing Pengcai Fine Chemical Co.) aqueous solution. The mixture was transferred into an autoclave and heated at 200 °C for 10 min to obtain ultrathin TiO_2 nanowires. The product was separated by centrifugation, rinsed with deionized water and ethanol and dried under vacuum, and then annealed at 450 °C for 2 h under an air atmosphere.

Preparation of TiO_2/ZnTe coaxial nanorods and ZnTe nanocrystals

Firstly, 11 mg of sodium tellurite (Na_2TeO_3, Sigma-Aldrich) and 4 mg of TiO_2 nanowires were added into 20 mL of deionized water and ultrasonicated for 10 min to form a homogeneous mixture. Then, 2 mL of hydrazine hydrate ($N_2H_4{\cdot}H_2O$, Nanjing Chemical Reagent Co.) and 6.8 mg of zinc chloride ($ZnCl_2$, Shanghai Xinbao Fine Chemical Co.) were sequentially dissolved in the mixture under vigorous stirring for 30 min. The mixture was transferred into an autoclave and heated at 140 °C for 4 h. The precipitates were washed with deionized water and ethanol and dried under vacuum, and then annealed at 300 °C for 2 h in air. The preparation of ZnTe nanocrystals was carried out in the same way as that of TiO_2/ZnTe coaxial nanorods, except no TiO_2 nanowires were added.

Preparation of TiO_2/ZnTe/Au nanocorncobs and TiO_2/Au nanowires

Briefly, 50 mg of TiO_2/ZnTe coaxial nanorods was dispersed in 50 mL of deionized water, and 1.0 mg of $HAuCl_4{\cdot}3H_2O$ was added into the mixture under ultrasonication. The resultant slurry was irradiated under a Xe-lamp (300 W, CEL-HXF300E, CEAULIGHT) for 2 h under vigorous stirring. The precipitates were collected by centrifugation, washed with deionized water and dried at 70 °C for 5 h. The preparation method of TiO_2/Au nanowires was similar, except TiO_2/ZnTe coaxial nanorods and light source were replaced by solely TiO_2 nanowires and ultraviolet light, respectively.

Characterization

The morphology of samples was identified by using a field-emission scanning electron microscope (FESEM, JSM-6480) and a transmission electron microscope (TEM, JEM-2100). The crystalline structures were acquired by using a powder X-ray diffractometer (XRD, Bruker D8 Advance) with a Cu Kα X-ray source. Raman analysis was performed on a Horiba JY-H800 spectrometer. XPS characterization was conducted by using a UlVAC VersaProbe PHI-5000 instrument with monochromatic Al Kα X-ray radiation. The PL spectra were collected using a home-built wide-field microscope[34] at an excitation wavelength of 405 nm after passing through a 425 nm long-pass filter (ET425lp, Chroma) and a transmission grating (Newport, 150 lines per mm) at 297 K. The time-resolved PL decays were measured using a single photon counting system (TCSPC, Picoharp 300) with 450 nm excitation light from a supercontinuous laser (Fianium SC-400). UV-Vis absorption spectra were taken by using a Shimadzu UV-3600 spectrophotometer.

Photocatalytic tests

Typically, 50 mg of the as-prepared photocatalyst was ultrasonically dispersed in 50 mL of deionized water in a reaction cell equipped with a top quartz glass and a gas circulation vacuum system (CEL-SPH2N, CEAULIGHT), and irradiated by using a 300 W Xe-lamp (350–800 nm, 96 mW cm^{-2}) under continuous stirring for 72 h. The temperature of the reaction cell was maintained at 6 °C throughout the test. The generated gas was analyzed by using a gas chromatograph (GC7900, Shanghai Techcomp).

STH energy conversion efficiency measurement of TiO_2/ZnTe/Au nanocorncobs under simulated sunlight

The STH efficiency was measured by irradiating 25 mg of the TiO_2/ZnTe/Au nanocorncob photocatalyst in 50 mL of deionized water under simulated solar irradiation supplied by a solar simulator (AM 1.5, SXDN-150E, Japan) for 6 h. The incident power was confirmed to be 100 mW cm^{-2} over the 7.1 cm^2 irradiation area. The total input energy was calculated as:

$$E_{Solar} = 0.1 \times 7.1 \times 6 \times 3600 = 1.53 \times 10^4 \text{ J}.$$

During the test, 630 μmol of H_2 was captured by using the gas chromatograph; thus the energy generated by water splitting is:

$$E_F = 630 \times 10^{-6} \times 6.02 \times 10^{23} \times 2.46 \times 1.609 \times 10^{-19} = 150 \text{ J}$$

where 2.46 eV is the free energy of water splitting. Thus, the STH efficiency of TiO_2/ZnTe/Au nanocorncobs is calculated to be:

$$\text{STH} = E_F/E_{Solar} = 150 \text{ J}/1.53 \times 10^4 \text{ J} = 0.98\%.$$

Photoelectrochemical tests

Photoelectrochemical experiments were performed with a CHI-760E electrochemical workstation using a conventional three-electrode system with an electrolytic cell (100 mL). A Pt wire electrode and a saturated calomel electrode (SCE) were used as the counter electrode and the reference electrode, respectively. To prepare the working electrode, 10 mg of the photocatalyst was firstly dispersed in 100 mL deionized water, and 10 μL of the as-prepared suspension was then dropped onto a RRDE or glassy carbon electrode (GCE) by using a micropipette and dried at room temperature to form a uniform catalyst layer. All tests were performed in pure water at open circuit voltage under darkness or Xe-lamp irradiation (350–800 nm, 96 mW cm^{-2}), respectively.

The electron transfer number during the reaction was measured by using a RRDE consisting of a Pt ring (5.0 mm inner-diameter and 7.2 mm outer-diameter) and a glassy carbon disk (4.0 mm diameter). The RRDE measurement was performed with a TiO_2/ZnTe/Au photocatalyst modified electrode in pure water under Xe-lamp irradiation at a rotating speed of 1600 rpm.

The electron transfer number (n) is calculated by the following formula:

$$n = 4I_{disk}/(I_{disk} + I_{ring}/N).$$

Herein, N, also called the RRDE collection efficiency, is determined to be 0.424 for this testing system. The values of I_{ring} and I_{disk} stand for the ring and disk currents.

EIS analysis was performed with a TiO_2/ZnTe/Au nanocorncob modified GCE electrode (5.0 mm diameter). The measurements were carried out under darkness and Xe-lamp irradiation by applying an AC voltage with 5 mV amplitude in a frequency range from 100 kHz to 100 mHz.

To explore the SPR effect of Au nanoparticles, PEC measurements were performed by using a three-electrode system with a photoelectrode as the working electrode, a Pt wire as the counter electrode and a SCE reference electrode in 1 M KOH aqueous solution. To prepare the working electrode, 3 mg of the sample was dispersed in 0.5 mL of ethanol and then spin-coated on the pre-treated ITO glass. Finally, the catalyst film on ITO glass was dried at 120 °C for 5 h before use. During photoelectrochemical testing, the electrolyte solution was first bubbled with N_2 for 1 h to exclude the dissolved oxygen. Then, linear sweep voltammetry (LSV) measurements of TiO_2 nanowires and TiO_2/Au nanowire photoanodes under darkness and light illumination of a 300 W Xe-lamp irradiation (350–800 nm, 96 mW cm^{-2}) coupled with a 550 nm monochromatic light optical filter were performed at a scan rate of 50 mV s^{-1}.

Z-scheme mechanism tests

The spin-trapping electron spin resonance (ESR) was used to detect active oxygen species ($^{\bullet}O_2^-$) and hydroxyl radicals ($^{\bullet}OH$) by using 5,5-dimethyl pyrroline *N*-oxide (DMPO) as the free radical trapping agent in methanol and aqueous solution, respectively. 2 mg catalyst was fully dispersed in 4 mL methanol or deionized water and 4 mL DMPO by stirring for 10 min at room temperature. The signals were recorded on an EMX-10/12 spectrometer (Brucker, Germany) in the dark and under light illumination.

Results and discussion

Fig. 1a–c show typical scanning electron microscopy (SEM) images of the as-prepared TiO_2/ZnTe/Au nanocorncob heterojunctions with a high aspect ratio, of which the diameter is approximately 50 nm and the length can be up to tens of micrometers. The TiO_2/ZnTe/Au nanocorncobs were prepared through a two-step strategy. Briefly, ultrathin TiO_2 nanowires were firstly prepared *via* a hydrothermal method. The TiO_2 nanowires possess an average diameter of ~15 nm, as observed by transmission electron microscopy (TEM, Fig. 1d). The high-resolution TEM (HRTEM) image in Fig. 1e shows that the ultrathin TiO_2 nanowires were grown along the (101) direction with a corresponding interplanar spacing of 0.35 nm. Subsequently, TiO_2/ZnTe coaxial nanorods were prepared by a hydrothermal process. Fig. 1g indicates that the as-prepared TiO_2/ZnTe coaxial nanorods have a typical core–shell structure, in which the TiO_2 nanowire was coated by a thick and rough shell assembled by large ZnTe nanocrystals. The selected-area electron diffraction (SAED) pattern (the inset of Fig. 1h) shows that the ZnTe shell has a cubic phase crystalline structure. The marked lattice fringe spacing of 0.35 nm in Fig. 1h can be well assigned to the (111) planes of zinc blende phase ZnTe. In the final synthesis step, uniform Au nanoparticles were decorated on the surface of TiO_2/ZnTe coaxial nanorods through the photoreduction of the $HAuCl_4 \cdot 3H_2O$ precursor (Fig. 1j). HRTEM characterization (Fig. 1k and l) reveals that Au nano-

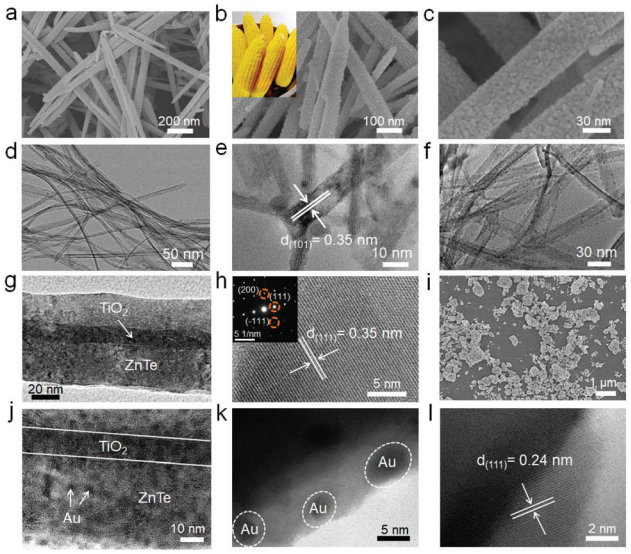

Fig. 1 Structural characterization of TiO_2/ZnTe/Au nanocorncobs, TiO_2 nanowires, Au/TiO_2 nanowires, TiO_2/ZnTe coaxial nanorods and ZnTe nanocrystals. (a–c) SEM images of TiO_2/ZnTe/Au nanocorncob heterojunctions. The inset of (b) shows a photograph of real corncobs. (d) TEM and (e) HRTEM images of TiO_2 nanowires. (f) TEM image of Au/TiO_2 nanowires. (g) HRTEM image of a TiO_2/ZnTe coaxial nanorod. (h) HRTEM image of the ZnTe outer shell of TiO_2/ZnTe coaxial nanorod. The corresponding SAED pattern in the inset of (h) reveals its crystalline nature. (i) SEM image of ZnTe nanocrystals. (j) HRTEM image of a TiO_2/ZnTe/Au nanocorncob. (k, and l) HRTEM images of Au nanoparticles decorated on the surface of TiO_2/ZnTe/Au nanocorncob heterojunctions.

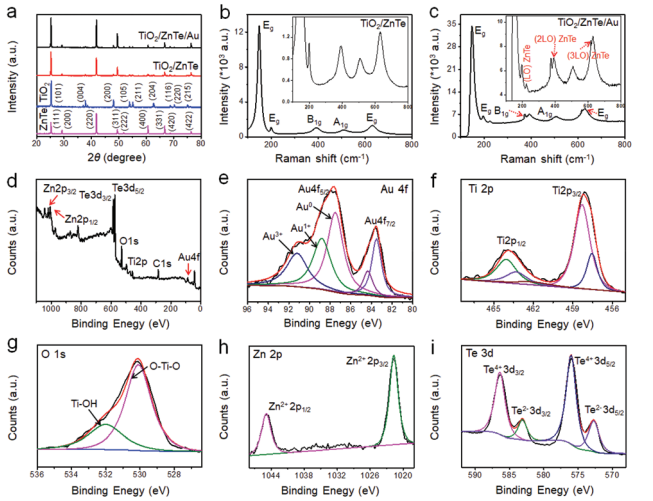

Fig. 2 Compositional characterization of TiO_2/ZnTe/Au nanocorncobs, TiO_2/ZnTe coaxial nanorods, TiO_2 nanowires and ZnTe nanocrystals. (a) XRD patterns of TiO_2/ZnTe/Au nanocorncobs (black), TiO_2/ZnTe coaxial nanorods (red), TiO_2 nanowires (blue) and ZnTe nanocrystals (pink), respectively. (b and c) Raman spectra of (b) TiO_2/ZnTe coaxial nanorods and (c) TiO_2/ZnTe/Au nanocorncobs with the magnified spectra in the insets. (d) Full XPS survey spectrum of TiO_2/ZnTe/Au nanocorncobs and corresponding high-resolution XPS spectra in (e) Au 4f region, (f) Ti 2p region, (g) O 1s region, (h) Zn 2p region and (i) Te 3d region, respectively.

particles with the size around 3–5 nm are homogeneously embedded on the surface of TiO_2/ZnTe coaxial nanorods. As shown in Fig. 1l, the observed adjacent lattice distance of 0.24 nm originates from the (111) planes of Au nanoparticles. As control samples, Au/TiO_2 nanowires (without ZnTe) (Fig. 1f) and pristine ZnTe nanocrystals (without Au and TiO_2) (Fig. 1i) were also prepared, as detailed in the Experimental section.

The compositions and crystallinity of the as-prepared samples were determined by powder X-ray diffraction (XRD). Fig. 2a shows that all diffraction peaks of ultrathin TiO_2 nanowires can be well indexed to anatase TiO_2 (JCPDS card No. 21-1272, space group: $I4_1/amd$). The control sample of ZnTe nanocrystals shows the characteristic peaks of (111), (200), (220), *etc.*, corresponding to cubic ZnTe (JCPDS card No. 15-0746) with high crystallinity. With the formation of the ZnTe shell on TiO_2 nanowires, the TiO_2/ZnTe coaxial nanorods exhibit well-resolved XRD peaks corresponding to anatase TiO_2 and cubic ZnTe, respectively, indicating that TiO_2 and ZnTe are successfully combined together to form a heterostructure. After the decoration of Au nanoparticles, the XRD pattern of TiO_2/ZnTe/Au nanocorncobs displays well-maintained peak densities, but negligible diffraction peaks of Au nanoparticles are observed since the weight content (~2 wt%) of Au is much lower than that of TiO_2 and ZnTe. Compared with TiO_2/ZnTe coaxial nanorods (Fig. 2b), the Raman spectrum of TiO_2/ZnTe/Au nanocorncobs (Fig. 2c) shows great enhancement in peak intensities, owing to the surface enhanced Raman scattering (SERS) from the SPR effect[35] of Au nanoparticles. Four main Raman peaks of TiO_2/ZnTe/Au nanocorncobs appear at 148, 392, 508 and 630 cm^{-1}, which can be assigned to the E_g, B_{1g}, A_{1g}, and E_g modes of anatase TiO_2,[36] respectively. The other three peaks at 206 cm^{-1} (LO mode), 412 cm^{-1} (2LO mode), and 618 cm^{-1} (3LO mode) (the inset of Fig. 2c) are derived from the ZnTe shell.[37] The elemental components of TiO_2/ZnTe/Au nanocorncobs were further identified by X-ray photoelectron spectroscopy (XPS), revealing the presence of Ti, O, Zn, Te and Au elements (Fig. 2d). Moreover, the high-resolution XPS spectra of different elements are shown in Fig. 2e–i, and the peaks can demonstrate the successful preparation of TiO_2/ZnTe/Au heterojunctions.

Fig. 3a and b show the photocatalytic overall water-splitting performances of different samples, including TiO_2/ZnTe/Au nanocorncobs, TiO_2/ZnTe coaxial nanorods, TiO_2/Au nanowires, and TiO_2 nanowires. The photocatalytic tests were conducted by dispersing 50 mg of photocatalyst in pure water without any sacrificial agents under the light irradiation of a 300 W Xe-lamp (350–800 nm, 96 mW cm^{-2} as verified by a light powermeter). The as-synthesized TiO_2/ZnTe/Au nanocorncobs and TiO_2/ZnTe coaxial nanorods exhibited good light-driven water-splitting activity with the generated molar ratio of H_2 and O_2 kept at 2 : 1. The H_2 evolution rate of TiO_2/ZnTe coaxial nanorods is *ca.* 2782.0 μmol g^{-1} h^{-1}. In comparison, the TiO_2/ZnTe/Au nanocorncob heterojunctions exhibited an increased H_2 production rate of 3344.0 μmol g^{-1} h^{-1}, indicating that the Au nanoparticles play a positive role for the enhanced photocatalytic water-splitting activity. However, no

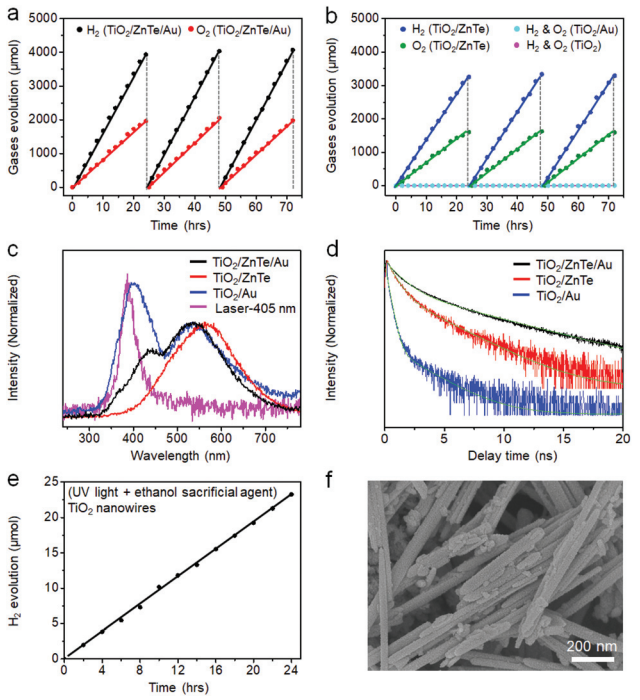

Fig. 3 Photocatalytic performances of TiO_2/ZnTe/Au nanocorncobs, TiO_2/ZnTe coaxial nanorods, Au/TiO_2 nanowires and TiO_2 nanowires. Photocatalytic H_2 and O_2 evolution performances of (a) TiO_2/ZnTe/Au nanocorncob heterojunctions, (b) TiO_2/ZnTe coaxial nanorods, TiO_2/Au nanowires and TiO_2 nanowires with the weights of 50 mg tested under a 300 W Xe-lamp irradiation (350–800 nm, 96 mW cm^{-2}) in pure water for 72 h. (c) PL spectra of TiO_2/ZnTe/Au nanocorncob heterojunctions, TiO_2/ZnTe coaxial nanorods and TiO_2/Au nanowires collected under an excitation wavelength of 405 nm. (d) Time-resolved PL decays of TiO_2/ZnTe/Au nanocorncob heterojunctions, TiO_2/ZnTe coaxial nanorods and TiO_2/Au nanowires collected under an excitation wavelength of 450 nm. (e) Photocatalytic H_2 evolution of TiO_2 nanowires (50 mg) under ultraviolet light irradiation (200–400 nm, 50 mW cm^{-2}) in mixed water/ethanol (3 : 1 in volume) solution for 24 h. (f) SEM image of TiO_2/ZnTe/Au nanocorncobs after photocatalytic water splitting under Xe-lamp for 72 h.

gas was detected when TiO_2/Au nanowires or pristine TiO_2 nanowires were used as the photocatalysts under the same testing conditions. This should be ascribed to the improper band structure, rapid electron–hole recombination and slow charge migration.[38] Moreover, the two-electron transfer process for H_2O_2 production and the reverse reaction of H_2O_2 into water might poison the TiO_2/Au and TiO_2 photocatalysts and suppress the water oxidation processes. The separation and recombination rates of photogenerated charge carriers of the samples have been investigated by photoluminescence (PL) spectroscopy. As shown in Fig. 3c, the broad emission peaks centered between 500 and 600 nm are observed for TiO_2/ZnTe/Au nanocorncob heterojunctions, TiO_2/ZnTe coaxial nanorods and TiO_2/Au nanowires, respectively, demonstrating that the energy levels of PL emissions are close to the bandgaps of the photocatalysts themselves. Note that the peaks that appeared before 450 nm (Fig. 3c) belong to the overlays of excitation light and PL signals. We further measured the time-resolved PL decays of these samples to study the charge carrier lifetimes. As shown in Fig. 3d, the average PL lifetime of TiO_2/ZnTe/Au nanocorncob heterojunctions (3.73 ns) is longer than those of TiO_2/ZnTe coaxial nanorods (1.76 ns) and TiO_2/Au nanowires (0.45 ns), indicating that the direct Z-scheme TiO_2/ZnTe/Au heterojunctions are favorable to facilitate the separation and transfer of photogenerated carriers. To further certify that the Z-scheme mechanism is the appropriate charge migration pathway for overall water splitting over the TiO_2/ZnTe/Au nanocorncob photocatalyst, ESR analysis was performed to detect the active oxygen species ($^{\bullet}O_2^-$) and hydroxyl radicals ($^{\bullet}OH$) produced on the surface of the catalyst by using DMPO as the free radical trapping agent. No ESR signals were observed in the dark while the characteristic peaks of DMPO-$^{\bullet}O_2^-$ and DMPO-$^{\bullet}OH$ appeared under light illumination (Fig. S2†). Therefore, $^{\bullet}OH$ and $^{\bullet}O_2^-$ produced under light irradiation confirm that the charge migration pathway for TiO_2/ZnTe/Au nanocorncobs follows the Z-scheme approach.[39] Meanwhile, the photocatalytic activity of TiO_2 nanowires under ultraviolet light irradiation (200–400 nm, 50 mW cm^{-2}) was evaluated by using ethanol aqueous solution (25% in volume) as the hole scavenger (Fig. 3e). The H_2 production rate of TiO_2 nanowires under ultraviolet light in ethanol solution (19.4 μmol g^{-1} h^{-1}) is much inferior to that of TiO_2/ZnTe/Au nanocorncobs in pure water, which indicates that TiO_2 itself is insufficient to achieve decent photocatalytic overall water-splitting activity. The TiO_2/ZnTe/Au nanocorncobs also show high stability during long-term tests. After the photo-reaction process of 72 h, the samples still maintain constant production rates of H_2 and O_2. The SEM image of TiO_2/ZnTe/Au nanocorncobs after a long-term photocatalytic reaction (Fig. 3f) shows that they well retain the original morphology, indicating their good durability. Moreover, the XRD pattern of TiO_2/ZnTe/Au nanocorncobs after the photocatalytic water splitting testing was also recorded (Fig. S1†). The crystalline structure and elementary composition of TiO_2/ZnTe/Au nanocorncobs have almost no change. Under simulated solar irradiation provided by an AM1.5 solar simulator (as detailed in the Experimental section), the STH energy conversion efficiency of TiO_2/ZnTe/Au nanocorncobs in pure water was found to be 0.98%, confirming the good photocatalytic performance among the reported representitative electrocatalysts (Table S1†). We propose that the combination of TiO_2/ZnTe heterojunctions and Au nanoparticles synergistically contributes to the enhanced photocatalytic overall water-splitting activity and stability of TiO_2/ZnTe/Au nanocorncobs.

The efficiency of photocatalytic overall water splitting is strongly dependent on the bandgap, the valence band (VB) and conduction band (CB) positions of the photocatalyst. Fig. S3a† and Fig. 4a show the UV-vis absorption spectra of different samples. To certify the SPR effect of Au nanoparticles, the UV-Vis absorption spectra of the TiO_2/Au nanowires and TiO_2 nanowires are first characterized in Fig. S3a.† The plasmon peak of the Au nanoparticles is located at ~550 nm, which would be helpful to enhance the sunlight-harvesting ability of the photocatalyst. Meanwhile, LSV curves of TiO_2

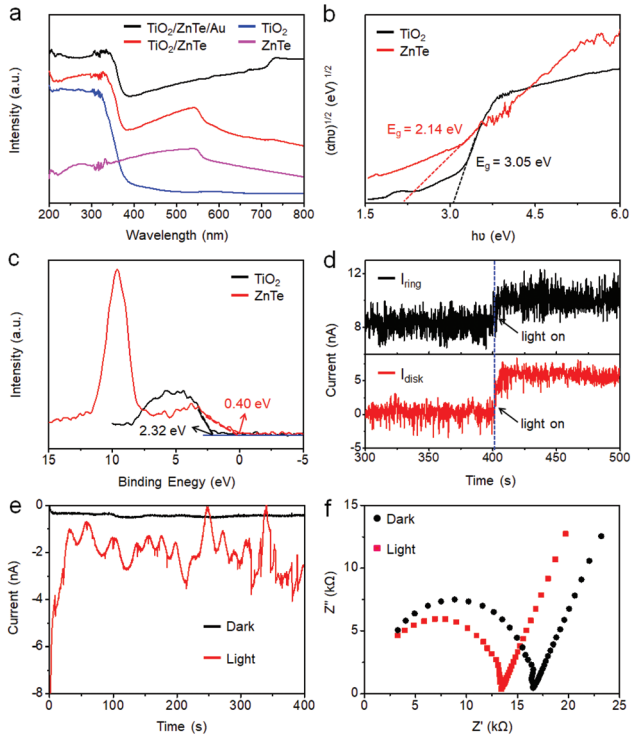

Fig. 4 Photochemical and photoelectrochemical characterization of TiO_2/ZnTe/Au nanocorncob heterojunctions. (a) UV-Vis spectra of TiO_2/ZnTe/Au nanocorncobs (black), TiO_2/ZnTe coaxial nanorods (red), TiO_2 nanowires (blue) and ZnTe nanoparticles (pink), respectively. (b) Band gap energies and (c) XPS valence spectra of TiO_2 nanowires and ZnTe nanoparticles, respectively. (d) Current–time curves of TiO_2/ZnTe/Au nanocorncobs recorded by the RRDE in pure water under darkness and Xe-lamp irradiation (350–800 nm, 96 mW cm^{-2}) at open-circuit voltage, respectively. (e) Chronoamperometry analysis of TiO_2/ZnTe/Au nanocorncobs measured with a standard three-electrode system at open-circuit voltage in pure water under darkness and Xe-lamp irradiation, respectively. (f) EIS analysis of TiO_2/ZnTe/Au nanocorncobs performed in pure water under darkness and Xe-lamp irradiation, respectively.

nanowires and TiO_2/Au nanowire photoanodes under darkness and 550 nm monochromatic light are shown in Fig. S3b.† TiO_2/Au nanowires show increased photocurrent during potential anodic sweeping and achieved prompt saturation of the photocurrent density under 550 nm monochromatic light illumination, suggesting photo-induced charge separation and collection on the photoanodes, whereas no photocurrent was observed by using TiO_2 nanowires. The result clearly demonstrates that the important SPR effect of the Au NPs contributed to the enhanced photocatalytic activity.[40,41] Due to the large bandgap of 3.05 eV, the TiO_2 nanowires mainly respond to ultraviolet light with the light absorption band edge at 406 nm (Fig. 4b). With the encapsulation of the ZnTe shell, the light absorption of TiO_2/ZnTe coaxial nanorods is extended to the visible light region due to the narrower bandgap of ZnTe (2.14 eV) (Fig. 4b). Analyzed from the XPS valence spectra in Fig. 4c, the VB positions of TiO_2 nanowires and ZnTe nanoparticles are found to be 2.32 eV and 0.40 eV, respectively; thus the CB positions of these two materials are estimated to be −0.73 eV and −1.74 eV, accordingly. After the decoration of Au nanoparticles, the TiO_2/ZnTe/Au nanocorncob heterojunctions show a greatly enhanced light response in the visible light region (Fig. 4a), resulting from the improved light absorption promoted by the strong SPR effect of Au nanoparticles.

To understand the photo-induced charge transfer process in the TiO_2/ZnTe/Au nanocorncob heterojunctions, rotating ring-disk electrode (RRDE) tests and chronoamperometry analysis were performed with a standard three-electrode setup in pure water under darkness and light illumination. According to the results of RRDE measurements (Fig. 4d), the electron transfer number n was found to be 2.26, as detailed in the Experimental section. It confirms that the photocatalytic water-splitting reaction promoted by TiO_2/ZnTe/Au nanocorncob heterojunctions is carried out through a two-electron/two-electron transfer process, which means that the H_2O molecule is firstly converted to the intermediate product of H_2O_2, and then H_2O_2 is rapidly decomposed to H_2O and O_2.[42] The standard redox potential of the H_2O/H_2O_2 couple is 1.78 V *vs.* standard hydrogen electrode (SHE), which is 550 mV higher than that of the O_2/H_2O couple (1.23 V), indicating that the formation of H_2O_2 is the rate-determining step during this reaction. Moreover, the obvious current oscillations in the *I–t* curve of chronoamperometry analysis under light illumination (Fig. 4e) adequately certify the H_2O_2 "generation-adsorption-decomposition" cycles. This demonstrates that H_2O is firstly oxidized to H_2O_2 on the surface of TiO_2/ZnTe/Au nanocorncobs *via* a two-electron reaction and then rapidly decomposed to O_2 during the subsequent oxygen evolution process. The negligible/no amount of H_2O_2 intermediate could be detected in the gas circulation vacuum system by using the TiO_2/ZnTe/Au photocatalyst after water oxidation, which can be verified by the colorimetric DPD method.[43–45] It further demonstrates that the stepwise $2e^-/2e^-$ two-step pathway could act as a desirable approach for water splitting by using TiO_2/ZnTe/Au nanocorncobs due to the absence of an unexpected poisoning effect of H_2O_2 on the photocatalyst surface, and thus TiO_2/ZnTe/Au could exhibit good photocatalytic activity and stability. Based on the above analysis, the photocatalytic water-splitting reaction on TiO_2/ZnTe/Au nanocorncobs can be described by the following stepwise charge transfer process:

$$TiO_2 + h\upsilon \rightarrow e_1^- + h_1^+ \quad (1)$$

$$ZnTe + h\upsilon \rightarrow e_2^- + h_2^+ \quad (2)$$

$$e_1^- + h_2^+ \leftrightarrow e_1^- \cdot h_2^+ \quad (3)$$

$$2H^+ + 2e_2^- \rightarrow H_2 \quad (4)$$

$$2H_2O + 2h_1^+ \rightleftharpoons H_2O_2 + 2H^+ \quad (5)$$

$$2H_2O_2 \rightarrow 2H_2O + O_2. \quad (6)$$

Briefly, the overall photocatalytic process of TiO_2/ZnTe/Au nanocorncob heterojunctions is depicted as follows: (i) under light illumination, photo-excited electron–hole pairs were formed on TiO_2 and ZnTe (eqn (1) and (2)). (ii) The photo-gen-

erated carriers were separated based on the direct Z-scheme mechanism, and a part of photo-excited electrons in TiO_2 could recombine with a part of holes in ZnTe (eqn (3)). (iii) The electrons in ZnTe that rapidly transferred and accumulated on Au nanoparticles served as "reservoirs", and the hydrogen evolution reaction was carried out (eqn (4)). (iv) The high-energy holes occupied on the surface of TiO_2 promote water oxidation and oxygen evolution through a two-electron/two-electron transfer process with H_2O_2 as the intermediate product (eqn (5) and (6)), which was verified from Fig. 4d and e. Owing to the higher reaction rate of the two-electron/two-electron water-splitting process, the photocatalytic system can realize higher efficiency and considerably low energy consumption for H_2 and O_2 production when compared to a conventional direct four-electron oxygen evolution process.[42]

As illustrated Fig. 5, the enhanced photocatalytic water-splitting performance of TiO_2/ZnTe/Au nanocorncobs shall be attributed to the following key factors: (i) the ZnTe semiconductor ($E_g \sim 2.14$ eV) can broaden the light absorption range to the visible light region and enhance the quantum efficiency. (ii) The appropriate direct Z-scheme heterojunction configuration between TiO_2 and ZnTe can improve the mobility of photo-induced carriers and retard the recombination of electron/hole pairs, thus enhancing the photocatalytic performance.[46] As a valid technique, electrochemical impedance spectroscopy (EIS) was performed to study the interfacial carrier transfer. Fig. 4f displays that the semicircle radius of TiO_2/ZnTe/Au nanocorncobs under illumination is smaller than that under darkness, indicating the lower carrier transfer resistance across the interface of the photocatalyst and electrolyte. This result reveals that the conductivity of TiO_2/ZnTe/Au nanocorncobs could be improved under light irradiation, owing to the generation of more charge carriers upon illumination. (iii) The presence of Au nanoparticles plays a dual role. As an efficient cocatalyst, Au nanoparticles decorated on the ZnTe shell formed a metal–semiconductor junction, namely, Schottky junction.[47] The Schottky junction can efficiently promote the migration of trapped electrons on TiO_2/ZnTe coaxial nanorods through Au nanoparticles to electron acceptors (H_2O or H^+), which benefits the hydrogen evolution reaction. On the other hand, Au nanoparticles with a strong SPR effect can take advantage of visible light and act as a helpful character in enhancing water-splitting activity. (iv) The rod-like TiO_2/ZnTe coaxial nanostructure with a large aspect ratio can ensure smooth charge transfer and suppress the recombination of electron/hole pairs. (v) The high dispersity and superb long-term stability of TiO_2/ZnTe/Au nanocorncobs contribute to the good photocatalytic stability and prevent the poisoning of generated H_2O_2 during the water oxidation process. In brief, the rational design of unique TiO_2/ZnTe/Au nanocorncob heterojunctions ensured enhanced light absorption and favorable charge migration during the water-splitting process.

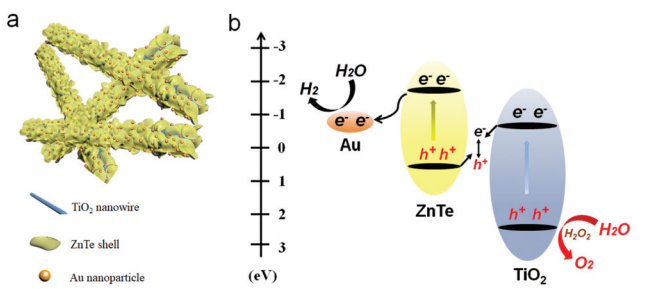

Fig. 5 Schematic illustration and the proposed mechanism of TiO_2/ZnTe/Au nanocorncob heterojunctions for photocatalytic overall water splitting. (a) Schematic illustration of TiO_2/ZnTe/Au nanocorncob heterojunctions. (b) The proposed mechanism for photocatalytic overall water splitting on direct Z-scheme TiO_2/ZnTe/Au nanocorncob heterojunctions.

Conclusions

In summary, we have successfully prepared a novel TiO_2/ZnTe/Au nanocorncob heterojunction photocatalyst *via* a facile solution-phase approach for high-efficiency overall water-splitting. The synergistic effects of TiO_2/ZnTe coaxial nanorods and Au nanoparticles greatly improved the photocatalytic performances for the sustainable hydrogen and oxygen generation with a stoichiometric ratio of 2 : 1 from pure water without any sacrificial reagents. The TiO_2/ZnTe/Au nanocorncobs exhibit high performance stability with a STH efficiency of 0.98%, much superior to pristine TiO_2 nanowires and TiO_2/ZnTe coaxial nanorods. Composed of available, non-toxic and stable materials, the well-designed TiO_2/ZnTe/Au photocatalyst represents a promising strategy to exploit clean hydrogen energy by utilizing sunlight and water.

Conflicts of interest

There are no conflicts to declare.

Acknowledgements

This work was supported by the National Key R&D Program of China (2017YFA0208200, 2016YFB0700600, and 2015CB659300), Projects of NSFC (21872069, 51761135104, and 21573108), Natural Science Foundation of Jiangsu Province (BK20180008, BK20150571, and BK20150583), High-Level Entrepreneurial and Innovative Talents Program of Jiangsu Province, and the Fundamental Research Funds for the Central Universities of China.

Notes and references

1 P. V. Kamat, *J. Phys. Chem. C*, 2007, **111**, 2834–2860.
2 A. Kudo and Y. Miseki, *Chem. Soc. Rev.*, 2009, **38**, 253–278.
3 K. Maeda and K. Domen, *J. Phys. Chem. Lett.*, 2010, **1**, 2655–2661.

4 Y. B. Wang, Y. S. Wang and R. Xu, *J. Phys. Chem. C*, 2013, **117**, 783–790.
5 Y. C. Lan, Y. L. Lu and Z. F. Ren, *Nano Energy*, 2013, **2**, 1031–1045.
6 H. Tong, S. X. Ouyang, Y. P. Bi, N. Umezaw, M. Oshikiri and J. H. Ye, *Adv. Mater.*, 2012, **24**, 229–251.
7 S. Q. Liu, Z. R. Tang, Y. G. Sun, J. C. Colmenares and Y. J. Xu, *Chem. Soc. Rev.*, 2015, **44**, 5053–5075.
8 J. Tian, Z. H. Zhao, A. Kumar, R. I. Boughton and H. Liu, *Chem. Soc. Rev.*, 2014, **43**, 6920–6937.
9 M. Z. Xie, X. D. Fu, L. Q. Jing, P. Luan, Y. J. Feng and H. G. Fu, *Adv. Energy Mater.*, 2014, **4**, 1300995.
10 K. Lalitha, G. Sadanandam, V. D. Kumari, M. Subrahmanyam, B. Sreedhar and N. Y. Hebalkar, *J. Phys. Chem. C*, 2010, **114**, 22181–22189.
11 K. K. Akurati, A. Vital, J. P. Dellemann, K. Michalow, T. Graule, D. Ferri and A. Baiker, *Appl. Catal., B*, 2008, **79**, 53–62.
12 D. R. Baker and P. V. Kamat, *Adv. Funct. Mater.*, 2009, **19**, 805–811.
13 H. J. Li, Y. Zhou, W. G. Tu, J. H. Ye and Z. G. Zou, *Adv. Funct. Mater.*, 2015, **25**, 998–1013.
14 S. S. K. Ma, K. Maeda, T. Hisatomi, M. Tabata, A. Kudo and K. Domen, *Chem. – Eur. J.*, 2013, **19**, 7480–7486.
15 X. W. Wang, G. Liu, Z. G. Chen, F. Li, L. Z. Wang, G. Q. Lu and H. M. Cheng, *Chem. Commun.*, 2009, **23**, 3452–3454.
16 F. Y. Xu, W. Xiao, B. Cheng and J. G. Yu, *Int. J. Hydrogen Energy*, 2014, **39**, 15394–15402.
17 W. C. Wang, S. Y. Chen, P. X. Yang, C. G. Duan and L. W. Wang, *J. Mater. Chem. A*, 2013, **1**, 1078–1085.
18 F. Lu, W. P. Cai and Y. G. Zhang, *Adv. Funct. Mater.*, 2008, **18**, 1047–1056.
19 W. W. He, H. K. Kim, W. G. Wamer, D. Melka, J. H. Callahan and J. J. Yin, *J. Am. Chem. Soc.*, 2014, **136**, 750–757.
20 X. J. Xu, L. F. Hu, N. Gao, S. X. Liu, S. Wageh, A. A. Al-Ghamdi, A. Alshahrie and X. S. Fang, *Adv. Funct. Mater.*, 2015, **25**, 445–454.
21 Y. P. Xie, Z. B. Yu, G. Liu, X. L. Ma and H. M. Cheng, *Energy Environ. Sci.*, 2014, **7**, 1895–1901.
22 J. Z. Chen, X. J. Wu, L. S. Yin, B. Li, X. Hong, Z. X. Fan, B. Chen, C. Xue and H. Zhang, *Angew. Chem.*, 2015, **127**, 1226–1230.
23 K. F. Wu, Z. Y. Chen, H. J. Lv, H. M. Zhu, C. L. Hill and T. Q. Lian, *J. Am. Chem. Soc.*, 2014, **136**, 7708–7716.
24 B. Mahler, V. Hoepfner, K. Liao and G. A. Ozin, *J. Am. Chem. Soc.*, 2014, **136**, 14121–14127.
25 Y. T. Liu, X. L. Zhang, R. H. Liu, R. B. Yang, C. B. Liu and Q. Y. Cai, *J. Solid State Chem.*, 2011, **184**, 684–689.
26 M. F. Ehsan, M. N. Ashiq and T. He, *RSC Adv.*, 2015, **5**, 6186–6194.
27 S. Jiao, Q. Shen, I. Mora-Seró, J. Wang, Z. X. Pan, K. Zhao, Y. Kuga, X. H. Zhong and J. Bisquert, *ACS Nano*, 2015, **9**, 908–915.
28 T. Tanaka, K. Saito, M. Nishio, Q. X. Guo and H. Ogawa, *Appl. Phys. Express*, 2009, **2**, 122101.
29 L. B. Luo, S. H. Zhang, R. Lu, W. Sun, Q. L. Fang, C. Y. Wu, J. G. Hu and L. Wang, *RSC Adv.*, 2015, **5**, 13324–13330.
30 Q. Wu, M. Litz and X. C. Zhang, *Appl. Phys. Lett.*, 1996, **68**, 2924–2926.
31 M. F. Ehsan and T. He, *Appl. Catal., B*, 2015, **166**, 345–352.
32 S. A. Rawool, M. R. Pai, A. M. Banerjee, A. Arya, R. S. Ningthoujam, R. Tewari, R. Rao, B. Chalke, P. Ayyub, A. K. Tripathi and S. R. Bharadwaj, *Appl. Catal., B*, 2018, **221**, 443–458.
33 J. T. Li, S. K. Cushing, P. Zheng, T. Senty, F. Meng, A. D. Bristow, A. Manivannan and N. Q. Wu, *J. Am. Chem. Soc.*, 2014, **136**, 8438–8449.
34 D. C. Hong, Y. P. Zhou, S. S. Wan, X. X. Hu, D. Q. Xie and Y. X. Tian, *ACS Photonics*, 2018, **5**, 2034–2043.
35 L. Brus, *Acc. Chem. Res.*, 2008, **41**, 1742–1749.
36 M. Kapilashrami, Y. F. Zhang, Y. S. Liu, A. Hagfeldt and J. H. Guo, *Chem. Rev.*, 2014, **114**, 9662–9707.
37 Y. H. Sun, Q. Zhao, J. Y. Gao, Y. Ye, W. Wang, R. Zhu, J. Xu, L. Chen, J. Yang, L. Dai, Z. M. Liao and D. P. Yu, *Nanoscale*, 2011, **3**, 4418–4426.
38 C. G. Silva, R. Juárez, T. Marino, R. Molinari and H. García, *J. Am. Chem. Soc.*, 2011, **133**, 595–602.
39 A. Hezam, K. Namratha, Q. A. Drmosh, D. Ponnamma, A. M. N. Saeed, V. Ganesh, B. Neppolian and K. Byrappa, *J. Mater. Chem. A*, 2018, **6**, 21379–21388.
40 X. K. Shao, B. X. Li, B. S. Zhang, L. Z. Shao and Y. M. Wu, *Inorg. Chem. Front.*, 2016, **3**, 934–943.
41 X. Zhang, Y. Liu, S. Lee, S. H. Yang and Z. H. Kang, *Energy Environ. Sci.*, 2014, **7**, 1409–1419.
42 J. Liu, Y. Liu, N. Y. Liu, Y. Z. Han, X. Zhang, H. Huang, Y. Lifshitz, S. T. Lee, J. Zhong and Z. H. Kang, *Science*, 2015, **347**, 970–974.
43 H. Bader, V. Sturzenegger and J. Hoigné, *Water Res.*, 1988, **22**, 1109–1115.
44 J. Y. Sheng, X. J. Li and Y. M. Xu, *ACS Catal.*, 2014, **4**, 732–737.
45 J. Jia, Q. Q. Zhang, Z. Li, X. Y. Hu, E. Z. Liu and J. Fan, *J. Mater. Chem. A*, 2019, **7**, 3828–3841.
46 T. Hisatomi, J. Kubota and K. Domen, *Chem. Soc. Rev.*, 2014, **43**, 7520–7535.
47 Y. J. Jang, J. W. Jang, J. Lee, J. H. Kim, H. Kumagai, J. W. Lee, T. Minegishi, J. Kubota, K. Domen and J. S. Lee, *Energy Environ. Sci.*, 2015, **8**, 3597–3604.